https://doi.org/10.5194/egusphere-2026-4682
Preprint. Discussion started: 6 August 2026

Vertical structure and controlling factors of cloud condensation nuclei activation over eastern China: Insights from aircraft measurements and interpretable machine learning

Yichen Lu[1], Honglei Wang[1,2*], Deyu Liu[1], Yue Chen[1], Chong Peng[3*], Can Song[3]

[1]Collaborative Innovation Center on Forecast and Evaluation of Meteorological Disasters (CIC-FEMD), China Meteorological Administration Aerosol-Cloud and Precipitation Key Laboratory, Nanjing University of Information Science & Technology, Nanjing, China

[2]State Key Laboratory of Atmospheric Environment and Extreme Meteorology, Institute of Atmospheric Physics, Chinese Academy of Sciences, Beijing, China

[3]Weather Modification Centre of Henan Province, Zhengzhou, 450000, China

Correspondence to: Honglei Wang (hongleiwang@nuist.edu.cn)

Abstract: Cloud condensation nuclei (CCN) play a critical role in cloud droplet formation and microphysical processes. Based on aircraft observations, this study investigated the factors controlling CCN number concentrations (NCCN) under different aerosol vertical structures (Decrease, Increase, and Stable) and supersaturation (SS) conditions using generalized additive models (GAM) combined with SHapley Additive exPlanations (SHAP).NCCN reached up to 10^3 cm^{-3} near the surface and generally decreased with altitude, while aerosol vertical structures modulated its abundance, with the Increase structure showing higher NCCN than Stable and Decrease structures. CCN activation ratios increased with SS and exhibited a non-monotonic vertical variation, with no consistent ranking among aerosol structures, indicating that supersaturation dominates CCN activation. Activated CCN droplet spectra showed unimodal distributions, with peak diameters increasing from ~2 μm at SS = 0.2 to ~5 μm at SS = 1.0. Although spectral shapes were similar among different structures, higher small-size aerosol concentrations (SA) enhanced CCN peak concentrations. GAM results identified temperature (T), SA, relative humidity (RH), and horizontal wind speed (WS) as important explanatory variables for NCCN variations, with contributions of 20%–56%, 9%–45%, 9%–40%, and 3%–19%, respectively. SHAP analysis revealed that the contributions of T varied among different aerosol vertical structures, showing positive associations under Decrease and Increase structures but negative associations under Stable conditions, whereas SA consistently exhibited positive contributions. RH showed nonlinear relationships with NCCN, with an inflection point near 60%.

https://doi.org/10.5194/egusphere-2026-4682
Preprint. Discussion started: 6 August 2026

1.Introduction

Aerosols influence cloud droplet formation by acting as cloud condensation nuclei (CCN), representing one of the key pathways of aerosol–cloud–climate interactions (Guo et al., 2021; Köhler, 1936; Tao et al., 2021a). Under certain supersaturation (SS) conditions, CCN can be activated to form cloud droplets, thereby affecting cloud droplet number concentration, effective radius, and microphysical structure, which in turn modify cloud radiative properties and precipitation efficiency. For instance, an increase in aerosols leads to higher CCN concentrations; if the cloud water content remains constant, this results in smaller droplet sizes, higher cloud droplet number concentrations, and increased cloud albedo (Lin et al., 2026; Twomey, 1977). Simultaneously, reduced droplet coalescence prolongs cloud lifetime and decreases precipitation (Albrecht , 1989; Khatri et al., 2023). These phenomena are referred to as the first and second indirect effects of aerosols. With the advancement of research, new insights have emerged. For example,(Prabhakaran et al., 2025) found that under a warming climate, aerosol perturbations affect the stratocumulus-to-cumulus transition (SCT) over the northeastern Pacific; during the non-precipitating stratocumulus stage, the cloud radiative effect (CRE) responds more strongly to climate change than to aerosols, whereas after cloud breakup, aerosol effects become dominant. Khatri et al. (2022) reported that increased aerosols may enhance droplet collision–coalescence, leading to larger cloud droplets. Borys et al. (2003)observed that high anthropogenic aerosol concentrations significantly alter the microphysical structure of lower "feeder" layers in orographic clouds, suppressing or even entirely blocking the riming growth of snow particles, thereby reducing snow water equivalent precipitation rates. Therefore, a thorough understanding of CCN activation processes and controlling factors is crucial for elucidating aerosol indirect climate effects.

The activation of CCN depends not only on ambient supersaturation but also on aerosol size distribution, chemical composition, and mixing state (Jose et al., 2026; Tao et al., 2021b). In most atmospheric environments, particle size distribution is a decisive factor for CCN activation, with larger particles more readily activated at lower supersaturation (Asa-Awuku et al., 2007; Kleinheins et al., 2025). According to Köhler theory, the critical supersaturation of an aerosol particle is closely related to its size and solubility; therefore, aerosol size spectrum is a key determinant of CCN number concentration and activation characteristics. Moreover, aerosols and related environmental factors often exhibit pronounced vertical heterogeneity (Xu et al., 2022; Zhang et al., 2021) which may modulate CCN activation, yet the

https://doi.org/10.5194/egusphere-2026-4682
Preprint. Discussion started: 6 August 2026

underlying mechanisms remain incompletely understood.

Current studies on CCN characteristics primarily rely on ground-based observations, satellite retrievals, and aircraft measurements. Among these, aircraft observations uniquely provide vertical distributions of aerosols, meteorological variables, and cloud microphysical parameters, offering distinct advantages for investigating aerosol–cloud interactions. For example, Zhang et al. (2022) found that in the North China Plain, the vertical distribution of NCCN is jointly influenced by T structure, air mass origin, anthropogenic emissions, and topography. Xu et al. (2022) reported that in southern China, NCCN initially increases with height, peaking at ~1.3 km, before rapidly decreasing. Liu et al. (2025)demonstrated that CCN vertical distributions are shaped by boundary layer structure, air mass transport, and thermodynamic conditions, with aerosols at different altitudes participating in cloud droplet formation via vertical transport, significantly affecting droplet number concentration and size distribution. However, most existing studies focus on single altitudes or overall statistical relationships, and systematic investigations of how different vertical aerosol structures (e.g., increasing or decreasing with height) influence CCN activation remain limited.

Traditional approaches, often based on correlation analysis or idealized theoretical frameworks, struggle to capture the nonlinear coupling among multiple factors. In recent years, machine learning (ML) has increasingly been applied in atmospheric sciences, showing clear advantages in handling high-dimensional, multivariate data and identifying key driving factors. In aerosol–cloud interaction studies, ML methods can extract aerosol–cloud interaction signals from complex meteorological covariates, reducing uncertainties inherent in conventional statistical approaches (Chen et al., 2022). In CCN research, ML has been used to predict NCCN based on aerosol chemical composition and meteorological variables, significantly improving model simulation accuracy (Ren et al., 2025). Further studies indicate that ML can reveal intrinsic relationships among aerosol chemical composition, size distribution, and CCN activation (Nair et al., 2021). Additionally, interpretable ML methods, such as SHAP, have been applied to quantitatively assess contributions of different factors to CCN and cloud microphysical parameters, providing critical insights into nonlinear mechanisms (Wang et al., 2025; Zipfel et al., 2024).

Against this background, the present study utilizes aircraft observations to systematically analyze CCN activation characteristics over eastern China, focusing on vertical and size distributions as well as variations under different cloud microphysical conditions. Machine learning methods are further employed to quantitatively evaluate key factors controlling CCN activation. This study enhances

https://doi.org/10.5194/egusphere-2026-4682
Preprint. Discussion started: 6 August 2026

understanding of aerosol–cloud interactions in eastern China and provides observational evidence to improve related parameterizations in climate models.

2.Data and Methods

2.1. Overview of Aircraft Observations

This study utilized data from four aircraft flights, including one calibration flight conducted by B-3726 and three observation flights by B-3435. Among all flight missions, Flight 1 (F1) was conducted under clear-sky conditions, while Flights 2–4 (F2–F4) sampled mixed-phase clouds. In particular, the cloud base heights were approximately 2300 m in F3 and F4. Additional flight details are provided in Table 1.

Table1. Detailed Information of Aircraft Flight Missions

Flight	Aircraft Modle	Date	Takeoff Time	Cloud Phase	0°C Level Height	Departure Location
1	B-3726	2018-3-21	21:44	Clear-sky	-	-
2	B-3435	2018-3-23	20:48	Mixed-phase	3500m	Zhengzhou
3	B-3435	2018-3-24	13:55	Mixed-phase	2600m	Xinzheng Airport
4	B-3435	2018-3-26	16：00	Mixed-phase	3100m	Xinzheng Airport

As shown in Fig.1, after taking off from Zhengzhou, F2 sampled altitudes between 1800 m and 4500 m, with in-cloud measurements around 4000 m (cloud identification criteria are detailed in Section 2.3). F3 sampled altitudes from 2400 m to 4200 m, with limited in-cloud data obtained around 2300 m. During F4, the sampling altitude ranged from 2200 m to 6000 m, where relatively deep clouds were observed.

https://doi.org/10.5194/egusphere-2026-4682
Preprint. Discussion started: 6 August 2026

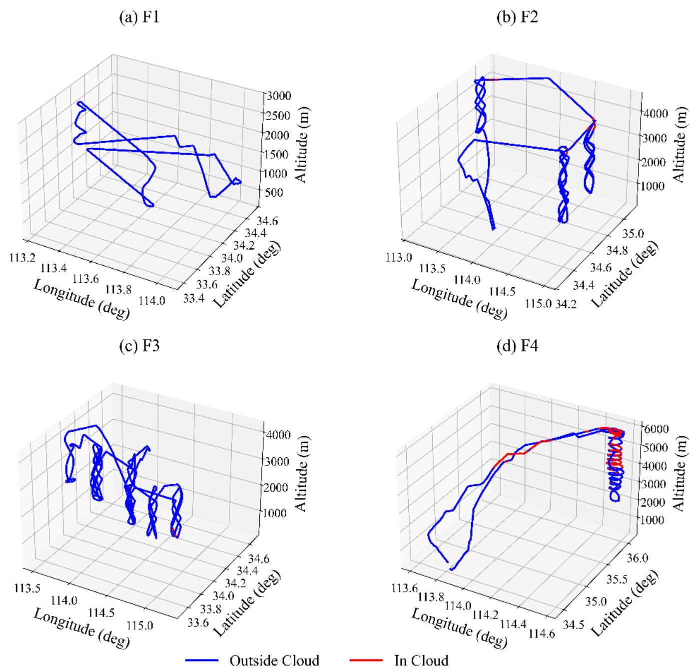

Fig.1. Flight trajectories of the four observation missions (March 21, 23, 24, and 26 correspond to F1–F4, respectively).

2.2. Instruments and Data Processing

The observations in this study were obtained using a Cloud Condensation Nuclei Counter (CCNC), Cloud Droplet Probe (CDP), Cloud Imaging Probe (CIP), Passive Cavity Aerosol Spectrometer Probe (PCASP), and the 20-Hz Aircraft Integrated Meteorology Measuring System (AIMMS-20). The core of the CCNC is a cylindrical thermal gradient diffusion chamber. A constant T gradient is applied along the walls of the chamber. Since heat diffuses more slowly through the air than through water vapor, a supersaturation is produced inside the cylinder. Aerosol flow is introduced into the centerline of the filtered and humidified sheath flow. A constant ratio of 10:1 is maintained between the sheath and aerosol flow. Supersaturation is developed inside the chamber according to the chamber flow, the streamwise T gradient, and the absolute pressure inside the column. Those particles whose critical supersaturation is less than the instrument supersaturation will grow as cloud droplet (Jayachandran et al., 2017; Liu et al., 2020). Five supersaturation levels (0.2%, 0.4%, 0.6%, 0.8%, and 1.0%) were set in the experiment. Each

https://doi.org/10.5194/egusphere-2026-4682
Preprint. Discussion started: 6 August 2026

measurement cycle lasted 25 min, with a sampling time of 5 min at each supersaturation level. Since the CCNC requires a finite response time to reach a stable supersaturation after switching between different supersaturation settings, transient periods around supersaturation transitions were excluded. The first and last 60 s of each supersaturation period were removed, and only the stable measurement period was retained for subsequent analysis(Jayachandran et al., 2017; Lance et al., 2006). The CDP provides comprehensive information on cloud droplet number concentration, size distribution, and liquid water content for droplets ranging from 2 to 50 μm (Faber et al., 2018). By guiding cloud droplets into the probe, the CDP determines the diameter of individual liquid droplets based on single-particle light scattering principles (Ke et al., 2024). The CIP quantifies ice particle concentration (Ni) and particle morphology by imaging particles passing through a collimated laser beam (Baumgardner et al., 2001). The PCASP measures particle size distribution based on the intensity of scattered light generated as individual particles pass through a laser beam, using the known relationship between scattering intensity and particle diameter (Cai et al., 2013). AIMMS-20 is a meteorological measurement system that provides integrated and on-demand atmospheric data (Ke et al., 2024). Detailed instrument specifications are provided in Table 2.

Table2. Information of Aircraft-Borne Instruments

Instrument	Measured Variables	Sampling Range	Time Resolution	Channel/Bin	Manufacturer
CCNC	CCN number concentration (NCCN), activated droplet size distribution	0.75~10μm	1s	20	Droplet Measurement Technologies (DMT)
CDP	Cloud droplet size distribution	2~50μm	1s	30	Droplet Measurement Technologies (DMT)
CIP	Cloud particle	25~1550μm	1s	62	Droplet

https://doi.org/10.5194/egusphere-2026-4682
Preprint. Discussion started: 6 August 2026

	size distribution				Measurement Technologies (DMT)
PCASP	Aerosol size distribution	0.1~3μm	1s	30	Droplet Measurement Technologies (DMT)
AIMMS-20	Meteorological variables (T, RH, etc.)	-	1s	-	Advanced Airborne Measurement Solutions

In this study, NCCN, cloud droplet number concentration (Nc), ice crystal number concentration (Ni), and aerosol number concentration (Na) were calculated using the following formulas:

$$N_d = \int n(r)dr = \sum N_{c,i,a}$$

Here, Nd represents the total particle number concentration (particles cm^{-3}), and NCCN, Nc, Ni, and Na are obtained by summing the particle number concentrations across the different instrument channels.

2.3. In-Cloud Data Classification

Based on previous airborne cloud microphysical studies(Hobbs and Rangno, 1998; Hou et al., 2021; Lance et al., 2010), together with operational experience from weather-modification aircraft observations in China, in-cloud data were identified using a simplified criterion: a measurement was considered in-cloud if either the Nc >10cm^{-3} or the Ni>1L^{-1}.

During in-cloud measurements, the CCN counter may detect both activated cloud droplets and interstitial aerosol particles. Without dedicated instrumentation or specific correction procedures, these two particle populations cannot be reliably distinguished. Therefore, to minimize the influence of cloud droplet activation on the CCN measurements, all data identified as in-cloud according to the criteria described above were excluded from subsequent analyses.

https://doi.org/10.5194/egusphere-2026-4682
Preprint. Discussion started: 6 August 2026

2.4 GAM and SHAP

GAM are flexible regression models that account for the additive effects of predictor variables on the response, including their potential nonlinear relationships (Bi et al.,2022). By applying smooth functions to input features, GAM can effectively capture nonlinear dependencies. In meteorology and atmospheric sciences, GAM is widely used to model complex environmental data and can accurately describe the relationships between meteorological variables and atmospheric constituents (Annareddy et al.,2026). GAM were selected in this study because the primary objective was to quantify the nonlinear relationships between environmental factors and CCN activation rather than simply maximize predictive performance. Unlike some complex machine learning and deep learning approaches that primarily emphasize predictive performance and may suffer from limited interpretability, GAM provides an interpretable framework by describing the response variable as the sum of smooth functions of individual predictors. This characteristic allows us to identify the nonlinear response patterns and potential thresholds of CCN concentrations in response to meteorological conditions and aerosol properties. SHAP is a framework for interpreting predictions from complex models, assigning an importance value to each feature to help understand why a model produces a specific prediction(Lundberg et al., 2017). SHAP is based on the Shapley value concept from game theory, which extracts feature contributions to ensure fair and consistent explanations. In this study, GAM was combined with SHAP to analyze the relationships between meteorological factors, cloud microphysical properties, and CCN concentrations.

In this study, To improve model robustness and reduce the risk of overfitting, a backward stepwise elimination procedure was incorporated into the GAM framework. In each iteration, the least significant term ($p < 0.01$) was removed, and model performance was assessed using the Akaike Information Criterion (AIC). The final model was selected based on the lowest AIC while retaining only statistically significant predictors, ensuring a balance between model complexity and interpretability.

The dataset was randomly divided into training (80%) and testing (20%) sets using a fixed random seed (random state = 42). Model performance was evaluated using R^2.

For nonlinear interpretation, SHAP values were computed using a model-agnostic Kernel Explainer applied to the trained GAM. A background set of 100 training samples and 300 test samples were used for Monte Carlo-based approximation of feature contributions.

Two SHAP metrics were used in this study: the mean absolute SHAP value, representing global

https://doi.org/10.5194/egusphere-2026-4682
Preprint. Discussion started: 6 August 2026

feature importance, and the mean signed SHAP value, indicating the direction of each feature's impact on CCN concentration. The SHAP contribution percentage was calculated by normalizing the mean absolute SHAP values across all features.

To reduce multicollinearity among aerosol variables, total aerosol number concentration (Na) was excluded, while SA, MA, and LA were retained to represent size-resolved aerosol populations, improving interpretability and avoiding redundancy.

3. Results and Discussion

3.1 Influence of Different Aerosol Vertical Structures on CCN Vertical Profiles

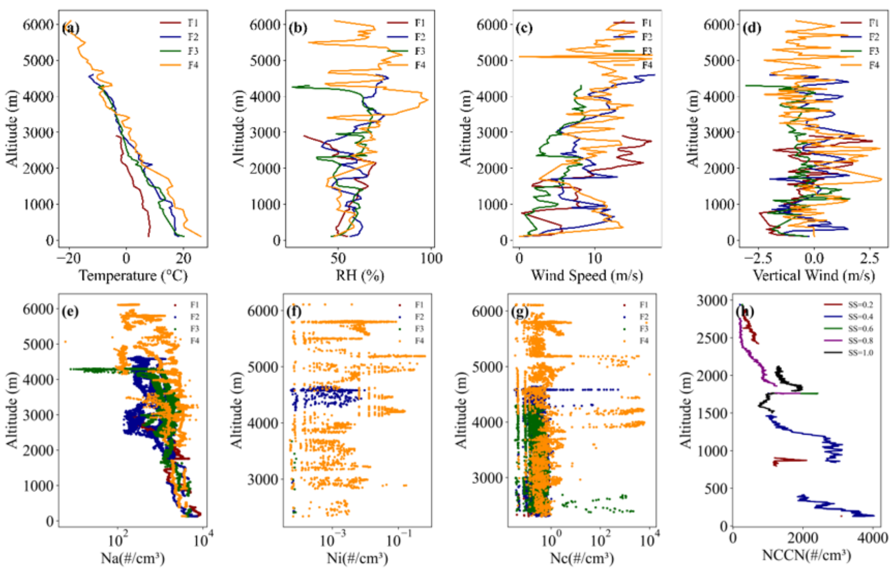

Fig.2. Vertical profiles of meteorological variables and particle concentrations for different flight missions. (a) Temperature; (b) Relative humidity; (c) Horizontal wind speed; (d) Vertical wind speed; (e) Aerosol number concentration; (f) Ice crystal number concentration; (g) Cloud droplet number concentration; (h) Variation of CCN number concentration with height under different supersaturation conditions during F1.

Figure 2 summarizes the vertical distributions of meteorological variables and particle concentrations during the four flight missions. T generally decreased with altitude, and no T inversion layer was observed. Near-surface T during F2–F4 exceeded 15 °C, whereas F1 exhibited relatively lower T of approximately 10 °C. RH generally increased with altitude in the lower atmosphere and decreased at higher levels, although F2 showed a more complex structure, with RH decreasing near 2000 m and increasing again around 2700 m. WS generally increased with altitude above 2000 m, while greater

https://doi.org/10.5194/egusphere-2026-4682
Preprint. Discussion started: 6 August 2026

variability was observed below this level. Vertical wind speed(VW) measurements indicated predominantly downward motions below 1000 m and stronger fluctuations aloft.

Na was highest near the surface, reaching the order of 10^4 cm^{-3}, and generally decreased with altitude (Fig.2e and Fig.S3–S6). Elevated Nc and Ni were observed in several flight missions. For example, F2 exhibited enhanced Nc and Ni near 4500 m, consistent with the cloud events identified around 21:30 and 22:00 (Fig.S4). Similar enhancements were also observed during F3 and F4 (Fig.2f,g and Fig.S5–S6), indicating the presence of cloud layers at different altitudes. According to the cloud classification criteria described in Section 2.3, these observations were used to identify in-cloud periods, which were subsequently excluded from the CCN analysis.

Fig.2h and Fig.S1 show that CCN number concentration (NCCN) reached values on the order of 10^3 cm^{-3} near the surface and generally exhibited decreasing vertical profiles under different supersaturation (SS) conditions, although local increases and nearly constant layers were also observed. For example, under SS = 0.4%, the NCCN profile during F1 exhibited a decrease–increase–decrease pattern with altitude. When observations from all flight missions were grouped by altitude and analyzed separately for each SS level (Fig.S2), CCN activation ratios generally exhibited an increase–decrease–increase pattern with altitude, reaching relatively low values around 4000 m in the composite profiles (3%–8% for SS $\leq$ 0.6 and 21%–35% for SS > 0.6). Activation ratios under SS $\geq$ 0.8% were generally higher than those under lower supersaturation conditions. In addition, under SS = 0.2%, 0.4%, and 1.0%, activation ratios decreased with altitude below approximately 500 m. It should be noted that the CCNC operated sequentially across different supersaturation levels during each flight, resulting in partial coupling between altitude and supersaturation. Therefore, the vertical variations presented here represent composite statistics from multiple flights rather than purely altitude-controlled or SS-controlled signals.

To investigate the impact of aerosol vertical structure on CCN activation characteristics, aerosol number concentration profiles were divided into consecutive vertical trend segments according to changes between adjacent altitude bins (Fig. S7). To reduce the influence of short-term fluctuations and measurement uncertainty, adjacent bins were classified as Stable when the absolute difference in aerosol number concentration was smaller than 100 cm^{-3} and the relative change was less than 20%. Segments exhibiting larger positive changes were classified as Increase, whereas those exhibiting larger negative changes were classified as Decrease. Segments were classified as Increase, Stable, or Decrease and subsequently grouped to represent different aerosol vertical structure categories.

https://doi.org/10.5194/egusphere-2026-4682
Preprint. Discussion started: 6 August 2026

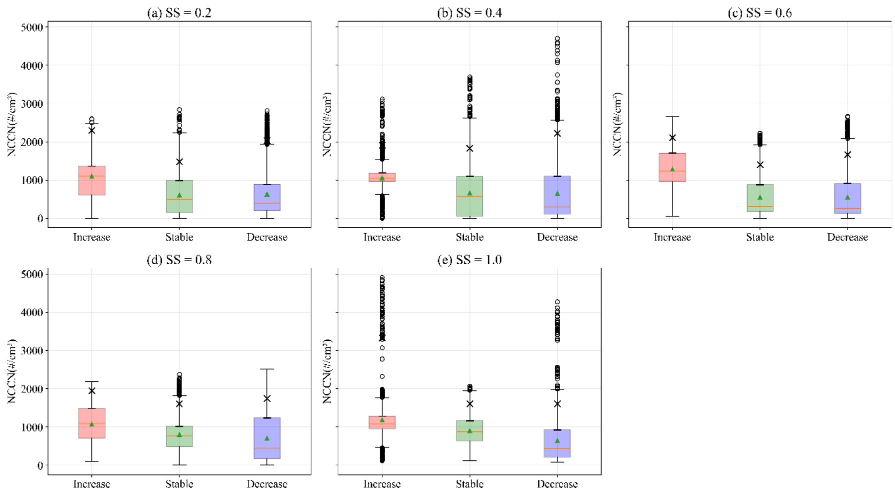

Fig.3. Distribution of cloud condensation nuclei (CCN) concentrations under different supersaturation (SS) conditions and aerosol vertical structural regimes. Boxplots illustrate CCN number concentrations (CCN NC) for three aerosol vertical structures (increasing, stable, and decreasing types) across five supersaturation levels (SS = 0.2, 0.4, 0.6, 0.8, and 1.0). The central line in each box represents the median value, while the box denotes the interquartile range (25th–75th percentiles). Whiskers extend to 1.5 times the interquartile range, and black circles indicate outliers. The triangle markers represent the arithmetic mean CCN concentration for each group. In addition, the 75th percentile (horizontal line) and 95th percentile (cross marker) are explicitly shown to highlight upper-tail behavior and distribution asymmetry under different aerosol structural and supersaturation conditions.

The statistical characteristics of NCCN and activation ratio under different aerosol vertical structure categories are further examined using boxplot analysis (Fig.3 and Fig.S8). The results show that NCCN exhibits generally higher median and mean values in the Increase category compared with the Stable and Decrease categories across most supersaturation conditions, indicating that aerosol vertical structure may influence the overall abundance of CCN. In contrast, CCN activation ratios show a strong dependence on supersaturation, with generally higher values under SS $\geq$ 0.8% compared to lower supersaturation conditions. However, differences among aerosol vertical structure categories are not consistently ordered across all SS levels, suggesting a condition-dependent rather than systematic structural control. Moreover, the interquartile range of activation ratios decreases with increasing supersaturation, indicating reduced variability and a more constrained activation state under high-SS conditions.

https://doi.org/10.5194/egusphere-2026-4682
Preprint. Discussion started: 6 August 2026

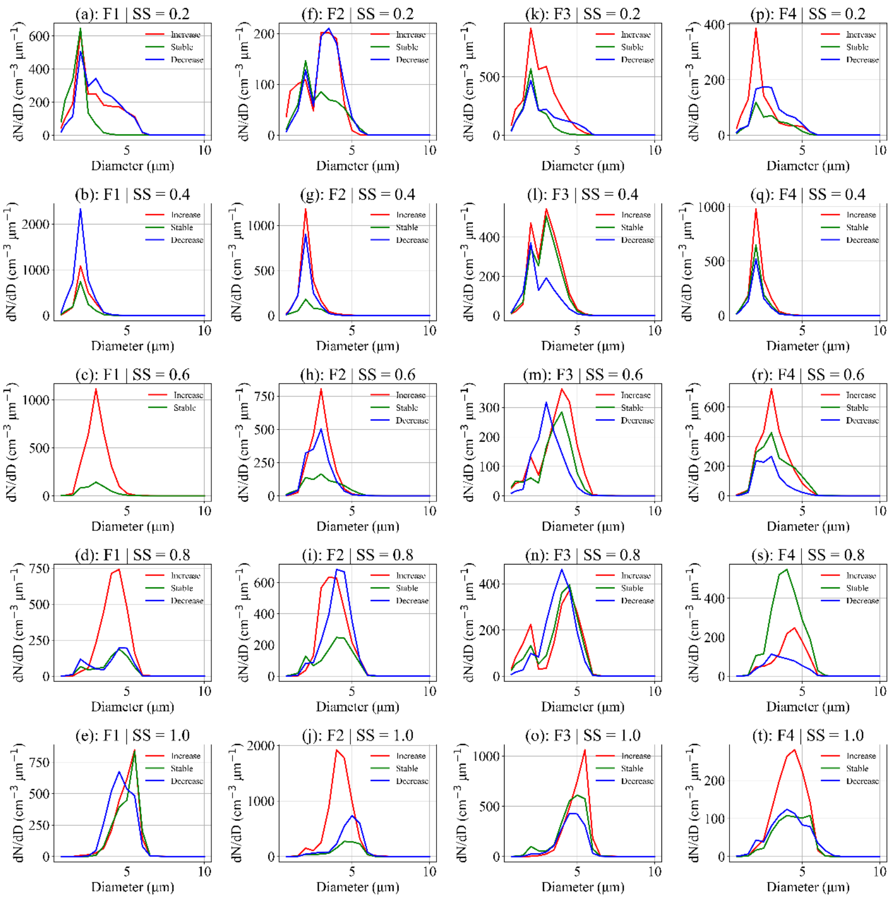

Fig.4. Size distributions of activated droplets measured by the CCNC under different supersaturation (SS) conditions and aerosol vertical structures for Flights F1–F4. Columns represent individual flight missions, and rows correspond to different SS conditions. Red, green, and blue curves denote the Increase, Stable, and Decrease aerosol vertical structures, respectively.

Fig. 4 shows that the size distributions of CCN-activated droplets measured by the CCNC are generally unimodal. The modal diameter is approximately 2 μm under low SS conditions (0.2 and 0.4), whereas it shifts to approximately 5 μm under higher SS conditions (0.8 and 1.0). This shift reflects differences in the subsequent condensational growth of activated droplets within the CCNC rather than changes in the critical activation diameter of aerosol particles. Under higher SS conditions, more aerosol particles with smaller sizes can be activated, and the enhanced water vapor supersaturation promotes faster condensational growth after activation, resulting in larger activated droplet sizes measured by the CCNC. For instance, in F1 (Fig. 4a–e), the modal diameter at SS = 0.2 is 2 μm for all three aerosol vertical structures, whereas it increases to 5.5 μm, 5.5 μm, and 4.5 μm at SS = 1.0 for the Increase, Stable,

https://doi.org/10.5194/egusphere-2026-4682
Preprint. Discussion started: 6 August 2026

and Decrease structures, respectively.

CCN-activated droplet spectra exhibit similar shapes among different aerosol vertical structures, with only minor differences in modal diameters and peak concentrations. For example, in Fig. 4q, the modal diameter is 2 μm for all three structures, with peak concentrations of 982, 646, and 519 cm^{-3} $μm^{-1}$ for the Increase, Stable, and Decrease structures, respectively. However, differences in CCN peak concentrations are not consistent among all cases. In Fig. 4b, the Decrease structure exhibits the highest peak concentration, while the Stable structure shows the lowest; in contrast, the opposite pattern is observed in Fig. 4s.

To further investigate the influence of vertical structure, the corresponding aerosol size distributions were analyzed (Fig.S9). Aerosol spectra generally exhibit a unimodal distribution consistent with the CCN-activated droplet spectra, with a peak around 0.14 μm, followed by a rapid decline beyond 0.32 μm. High concentrations of aerosols with diameters <1 μm correspond to higher CCN peak concentrations. For example, in Fig.S9p, the <1 μm aerosol concentration follows the order Increase > Decrease > Stable, which is consistent with the corresponding CCN-activated droplet spectra in Fig.4p Similar patterns are observed in other cases, suggesting that variations in <1 μm aerosol concentrations likely contribute to changes in CCN peak concentrations.

It should be noted that the CCN-activated droplet sizes measured by the CCNC reflect a continuous condensational growth process under prescribed supersaturation conditions, rather than an equilibrium particle size. Therefore, the retrieved droplet sizes may be sensitive to instrumental settings, CCN concentration, and water vapor supply conditions. Accordingly, interpretations of size-related variations should be made with appropriate caution.

Overall, the results indicate that CCN vertical distributions are jointly regulated by supersaturation, aerosol loading, and vertical structural characteristics. Supersaturation primarily controls the activation efficiency, resulting in consistently higher activation ratios under high-SS conditions, while aerosol vertical structure mainly modulates CCN availability through variations in aerosol abundance, particularly submicron particles.

However, the influence of vertical structure on activation ratios is not systematic across all supersaturation levels, suggesting a strong condition-dependent behavior rather than a purely structural control. These results further imply that CCN variability arises from coupled effects between aerosol population characteristics and environmental conditions, rather than a single dominant factor.

https://doi.org/10.5194/egusphere-2026-4682
Preprint. Discussion started: 6 August 2026

This motivates a more quantitative investigation of the relative roles of meteorological conditions and size-resolved aerosol properties in CCN formation, which is further addressed using correlation analysis, GAM modeling, and SHAP-based interpretation in the following sections.

3.2 Correlation Analysis between CCN Number Concentration and Environmental Factors under Different Supersaturation Conditions

Pearson correlation analysis was conducted to quantify the relationships between CCN number concentrations and environmental factors under different aerosol vertical structures and supersaturation conditions. Statistical significance was assessed using p-values, and correlation coefficients were reported to evaluate the strength and direction of these relationships. Figure 5 shows that, across different aerosol vertical structures, temperature (T), SA, and Na are generally positively correlated with CCN concentrations, whereas wind speed (WS), vertical wind (VW), medium-size aerosol number concentration (MA), and large-size aerosol number concentration (LA) exhibit predominantly negative correlations. RH shows an SS-dependent relationship, with negative correlations under low supersaturation conditions (SS = 0.2 and 0.4) but positive correlations at higher supersaturations (SS = 0.6, 0.8, and 1.0). Among all examined factors, T, SA, and Na exhibit the strongest correlations with CCN, followed by RH and WS, while VW, MA, and LA show relatively weaker relationships.

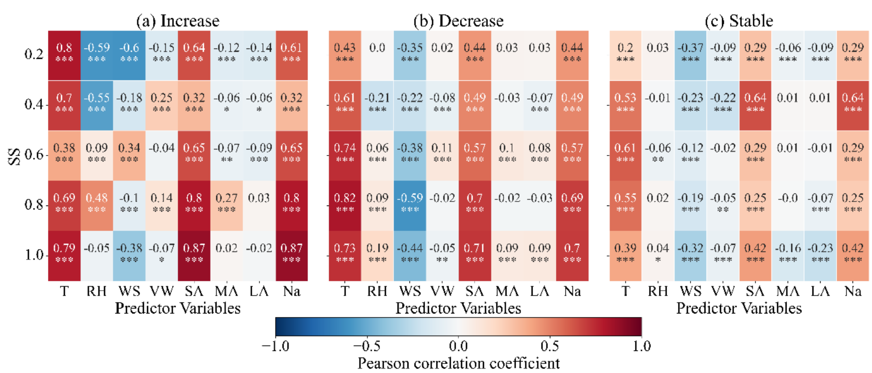

Fig.5.F1-F4 Correlation between CCN number concentration and various environmental factors under different aerosol vertical structures for Flights F1–F4 at multiple supersaturation (SS) conditions. Four meteorological variables and four aerosol size classes are included: small aerosols (SA, 0.1–1 μm), medium aerosols (MA, 1–2 μm), large aerosols (LA, 2–3 μm), and total aerosols (Na, 0.1–3 μm). Red and blue colors indicate positive and negative correlations, respectively, and the numerical values represent the correlation coefficients. Asterisks denote statistical significance (*p < 0.05, **p < 0.01, ***p < 0.001).

https://doi.org/10.5194/egusphere-2026-4682
Preprint. Discussion started: 6 August 2026

The overall correlation patterns are generally consistent among different aerosol vertical structures, although the correlation coefficients vary. In particular, correlations under the Stable structure are generally weaker than those under the Increase and Decrease structures. For example, T exhibits positive correlations with CCN under all three structures, with mean correlation coefficients of 0.456, 0.672, and 0.666 for Stable, Increase, and Decrease structures, respectively. Furthermore, relatively high correlation coefficients in the Increase structure mainly occur at SS = 0.2, 0.8, and 1.0, whereas those in the Decrease structure are primarily observed at SS = 0.8 and those in the Stable structure at SS = 0.4.

Notably, the correlations between Na and CCN are highly consistent with those between SA and CCN, with differences in correlation coefficients generally within 0.1. This suggests that variations in Na are largely associated with changes in SA, highlighting the importance of small-size particles in determining aerosol number concentration variability. This result is also consistent with the aerosol size distribution characteristics shown in Fig. S9.

3.3 Quantitative Analysis of Factors Influencing CCN Activation Based on GAM and SHAP Machine Learning Approaches

To further investigate the nonlinear effects of these factors on CCN number concentration and quantify their individual contributions, a GAM was employed in combination with the SHAP method. This approach enables the assessment of the relative importance of each factor and elucidates their underlying mechanisms. Model evaluation results indicate that the mean R^2 values for the training and test sets are 0.85 and 0.82, respectively, demonstrating good model fit and generalization performance. The relationship between predicted and observed NCCN values (Fig.S10) shows that most data points are distributed near the 1:1 reference line, indicating strong agreement between model predictions and observations, consistent with the high R^2 values.

https://doi.org/10.5194/egusphere-2026-4682
Preprint. Discussion started: 6 August 2026

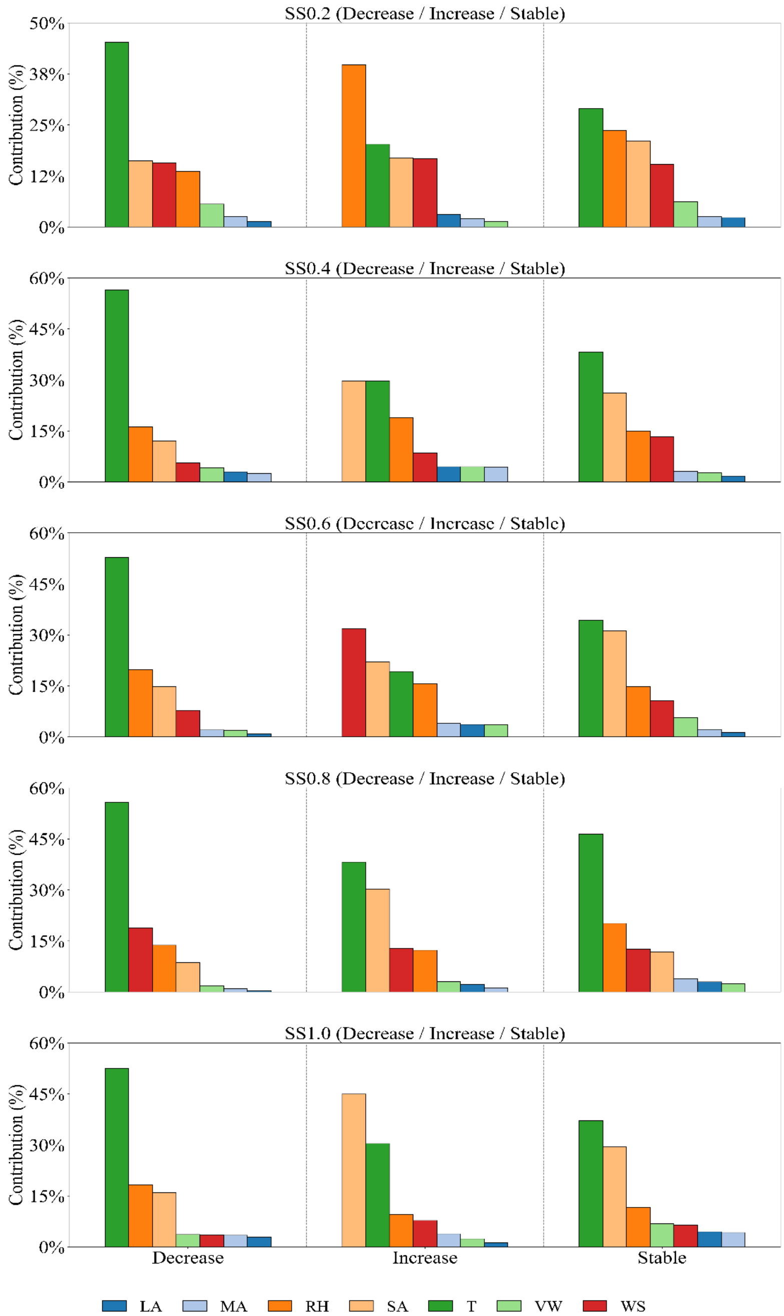

Fig.6. |SHAP| contribution rates of different factors to CCN number concentration under varying aerosol vertical structures and supersaturation conditions.

Fig.6 shows that under the three aerosol vertical structures, T, RH, WS and SA consistently rank among the top four contributors, indicating their strong contributions to variations in NCCN within the model framework. Specifically, in the Decrease and Stable scenarios, T exhibits the highest contribution, exceeding 25% in both cases. In the Increase scenario, T's contribution ranking decreases under certain SS conditions but still remains above 15%, suggesting that T maintains high importance across different scenarios and is closely associated with variations in NCCN. RH contributes approximately 15% on average, reaching up to 38% in certain scenarios. WS contributes around 12% on average, peaking at approximately 30% under SS = 0.6 in the Increase scenario, indicating a scenario-dependent influence of RH and WS. This may relate to the effect of humidity on aerosol hygroscopic growth and the role of WS in aerosol transport and dispersion. SA generally shows high contributions across most scenarios, with contribution rates often exceeding 15%.

In contrast, VW contributes less than 10%, indicating a relatively minor impact on NCCN. MA and LA also contribute less than 10%, much lower than SA, suggesting that the contribution of aerosols to NCCN is primarily driven by SA, consistent with previous analyses.

Moreover, the SHAP net contributions of NCCN exhibit notable differences under varying aerosol vertical structures and supersaturation conditions (Fig.S11). The net contributions of T, RH, WS and SA generally have larger absolute values, whereas those of VW, LA and MA are relatively smaller, consistent with the previously discussed contribution rates. Specifically, T shows predominantly positive contributions under the Decrease and Increase scenarios, but mainly negative contributions under the Stable scenario. SA contributes positively across all three scenarios, while the directions of WS and RHcontributions do not show clear scenario-dependent patterns.

In summary, the model identifies T (20%–56%), SA (9%–45%), RH (9%–40%), and WS (3%–19%) as the most important factors under most scenarios, whereas LA, MA, and VW only show significant contributions in specific cases. Analysis of the individual SHAP value variations (Fig.S12–S29) further reveals that, the SHAP values of T, RH, WS, VW, and SA generally exhibit pronounced nonlinear behavior across different scenarios, while those of LA and MA vary approximately linearly.

The contribution of T generally increases with its magnitude; in the high range, it usually shows positive SHAP values, whereas in the low range it shows negative SHAP values. This indicates that the model considers higher T conditions favorable for an increase in NCCN, while lower T conditions are unfavorable. Comparing the vertical distributions of T and Na (Fig.2 and Fig.S7) reveals a certain similarity: high (low) T values often correspond to higher (lower) Na concentrations. Therefore, the

https://doi.org/10.5194/egusphere-2026-4682
Preprint. Discussion started: 6 August 2026

contribution of T to NCCN in the model may partly reflect the coordinated variation between T and Na distributions, rather than implying that T alone directly controls CCN formation.

The contribution of SA generally increases with its magnitude, showing a significant positive effect on NCCN at high values. This may be because small particles can grow through condensation or coagulation into the accumulation mode, becoming effective cloud condensation nuclei. Previous studies have shown that small particles produced by new particle formation can significantly increase CCN concentrations during subsequent growth (Kerminen et al., 2012). Therefore, an increase in SA may reflect an enhanced potential source of CCN, resulting in a positive contribution in the model.

The SHAP values of RH exhibit a pronounced nonlinear relationship with CCN concentrations. An inflection point is observed around 60% RH in most cases. Below this level, SHAP values generally increase with increasing RH, suggesting that higher humidity conditions favor aerosol water uptake and enhance CCN activation. Above this level, the SHAP contribution gradually decreases, indicating that the marginal influence of further RH increases on CCN concentrations becomes weaker, possibly because particles have already undergone substantial hygroscopic growth under humid conditions.

The contribution of WS to NCCN SHAP values varies considerably across different scenarios, showing a strong dependence on environmental conditions.

The contributions of other factors show relatively small changes or large variations depending on the scenario, and are therefore not discussed in detail in this study.

4.Conclusions

NCCN reaches up to 10^3 cm^{-3} near the surface and generally decreases with increasing altitude. Under different supersaturation (SS) conditions, the CCN activation fraction exhibits a "first increase–then decrease–then increase" variation with height, reaching a minimum around 4000 m (3%–8% for SS $\leq$ 0.6 and 21%–35% for SS > 0.6). Overall, higher activation fractions were observed under SS $\geq$ 0.8, consistent with the expected dependence of CCN activation on supersaturation.

Based on the vertical variation characteristics of aerosol number concentration, the altitude layers are classified into Decrease, Increase, and Stable types, and all segments within each category are combined for statistical analysis. The results show that NCCN differs significantly among different aerosol vertical structures, with the Increase structure exhibiting higher NCCN overall than the Stable and Decrease structures, indicating that aerosol vertical structure may modulate the overall CCN

https://doi.org/10.5194/egusphere-2026-4682
Preprint. Discussion started: 6 August 2026

concentration distribution. In contrast, CCN activation ratios do not show a consistent ranking among different vertical structures, but are substantially higher under SS ≥ 0.8%, indicating a stronger dependence on supersaturation.

The CCN-activated droplet spectra generally exhibit a unimodal distribution. At SS = 0.2, the modal diameter is approximately 2 μm, increasing to about 5 μm as SS rises to 1.0. Although the spectral shape is broadly similar across different aerosol vertical structures, with relatively small differences in modal diameter, variations in peak concentration are observed. In general, higher SA correspond to higher CCN peak concentrations.

T, SA, and Na are consistently positively correlated with CCN, whereas WS, VW, MA, and LA are mainly negatively correlated. RH shows negative correlations under low supersaturation (SS = 0.2 and 0.4) and positive correlations under higher supersaturation (SS = 0.6, 0.8, and 1.0). Overall, T, SA, and Na exhibit the strongest correlations with CCN, followed by RH and WS, while VW, MA, and LA show weaker correlations. Correlations under the Stable structure are generally weaker than those under the Increase and Decrease structures.

GAM and SHAP analyses indicate that T, SA, RH, and WS are identified as the most important predictors associated with NCCN variations in the model, with contribution rates of approximately 20%–56%, 9%–45%, 9%–40%, and 3%–19%, respectively. In the Increase structure, the contribution of T is somewhat reduced. T contributes positively in the Decrease and Increase structures but negatively in the Stable structure. SA contributes positively across all three aerosol vertical structures, whereas WS and RH do not exhibit clear scenario-dependent patterns in their net contributions. In addition, SHAP results show that T, RH, WS, VW, and SA exhibit pronounced nonlinear responses, whereas LA and MA show approximately linear behavior.

The contributions of T and SA generally increase with their magnitude, showing significant positive SHAP contributions at high values. RH exhibits a pronounced nonlinear characteristic, with a turning point around 60%: below this threshold, SHAP values increase with RH, while above it, they gradually decrease. The contribution of WS varies considerably across different scenarios, showing a strong dependence on environmental conditions.

Overall, the dominant roles of temperature and fine aerosol concentration identified in this study are generally consistent with previous observational and numerical studies showing that thermodynamic conditions and aerosol properties jointly regulate CCN activation(Thomas et al., 2024). Unlike previous

https://doi.org/10.5194/egusphere-2026-4682
Preprint. Discussion started: 6 August 2026

numerical studies, particularly direct numerical simulations (DNS), which mainly investigate CCN activation under idealized cloud conditions, this study provides aircraft-based observational evidence of CCN variability and its controlling factors under realistic atmospheric environments. These complementary observational results provide useful constraints for improving our understanding of aerosol–cloud interactions.

Several limitations should be acknowledged. First, CCN measurements at different supersaturation levels were conducted sequentially rather than simultaneously, which may introduce partial coupling between altitude and supersaturation despite the quality-control procedures applied. Second, the analyses were based on four aircraft flights over eastern China and therefore may not fully represent the variability under different meteorological conditions or in other regions. Future studies combining long-term aircraft observations with numerical simulations are needed to further evaluate the generality of these findings and the underlying physical mechanisms.

In addition, some predictor variables, particularly temperature and altitude, are physically correlated in aircraft observations. Consequently, although GAM and SHAP identify temperature as one of the most influential predictors, the model quantifies statistical associations rather than direct causal relationships. Future studies incorporating more independent observations and process-based numerical simulations are needed to further distinguish the respective influences of thermodynamic conditions and altitude-related variability.

Despite these limitations, the present results suggest that variations in lower-tropospheric NCCN are closely associated with aerosol loading, thermodynamic conditions, and aerosol vertical structure. The combination of aircraft observations with interpretable machine learning provides an effective framework for identifying the dominant environmental factors associated with CCN variability and offers valuable observational constraints for improving CCN activation parameterizations in cloud-resolving models as well as larger-scale atmospheric models.

Code and data availability

Code and data will be made available on request.

https://doi.org/10.5194/egusphere-2026-4682
Preprint. Discussion started: 6 August 2026

Author contributions

Yichen Lu conducted the conceptualization of the study, performed data curation, formal analysis, validation, and investigation, and was responsible for manuscript preparation, including writing the original draft and revising the manuscript. Honglei Wang contributed to the methodology development, supervised the research, acquired funding, and revised the manuscript. Deyu Liu and Yue Chen contributed to methodology development and software implementation. Chong Peng and Can Song contributed to data curation and provided resources. All authors reviewed and approved the final version of the manuscript.

Competing interests

The contact author has declared that none of the authors has any competing interests.

Acknowledgements

This study was supported by the Science & Technology Fundamental Resources Investigation Program (Grant No. 2025FY101504), the Key Science and Technology Project of Henan Province (252102321006), and Open Research Fund Project of State Key Laboratory of Atmospheric Environment and Extreme Meteorology. The authors gratefully acknowledge the Weather Modification Centre of Henan Province, Zhengzhou 450000, China, for providing the aircraft observation data used in this study. The authors also express their sincere appreciation to the aircraft observation crew for their dedicated efforts, professional support, and valuable contributions throughout the field campaigns.

Financial support

This study was supported by the Science & Technology Fundamental Resources Investigation Program (Grant No. 2025FY101504), the Key Science and Technology Project of Henan Province (252102321006), and Open Research Fund Project of State Key Laboratory of Atmospheric Environment and Extreme Meteorology.

https://doi.org/10.5194/egusphere-2026-4682
Preprint. Discussion started: 6 August 2026

References

Albrecht, B.A., 1989. Aerosols, Cloud Microphysics, and Fractional Cloudiness. Science 245, 1227–1230. https://doi.org/10.1126/science.245.4923.1227

Annareddy, R.R., Shaik, F.B., Thatapi, B., Chukkaluri, C.R., Yadiki, N.A., 2026. Source attribution and temporal patterns of surface ozone in a semi-arid region of southern India via GAM and trajectory models. J. Atmos. Sol.-Terr. Phys. 278, 106699. https://doi.org/10.1016/j.jastp.2025.106699

Asa-Awuku, A., Nenes, A., Sullivan, A.P., Hennigan, C.J., Weber, R.J., n.d. Investigation of molar volume and surfactant characteristics of water-soluble organic compounds in biomass burning aerosol.

Baumgardner, D., Jonsson, H., Dawson, W., O'Connor, D., Newton, R., 2001. The cloud, aerosol and precipitation spectrometer: a new instrument for cloud investigations. Atmos. Res., 13th International Conference on Clouds and Precipitation 59–60, 251–264. https://doi.org/10.1016/S0169-8095(01)00119-3

Bi, Z., Ye, Z., He, C., Li, Y., 2022. Analysis of the meteorological factors affecting the short-term increase in O3 concentrations in nine global cities during COVID-19. Atmos. Pollut. Res. 13, 101523. https://doi.org/10.1016/j.apr.2022.101523

Borys, R.D., Lowenthal, D.H., Cohn, S.A., Brown, W.O.J., 2003. Mountaintop and radar measurements of anthropogenic aerosol effects on snow growth and snowfall rate. Geophys. Res. Lett. 30. https://doi.org/10.1029/2002GL016855

Cai, Y., Snider, J.R., Wechsler, P., 2013. Calibration of the passive cavity aerosol spectrometer probe for airborne determination of the size distribution. Atmos. Meas. Tech. 6, 2349–2358. https://doi.org/10.5194/amt-6-2349-2013

Chen, Y., Haywood, J., Wang, Y., Malavelle, F., Jordan, G., Partridge, D., Fieldsend, J., De Leeuw, J., Schmidt, A., Cho, N., Oreopoulos, L., Platnick, S., Grosvenor, D., Field, P., Lohmann, U., 2022. Machine learning reveals climate forcing from aerosols is dominated by increased cloud cover. Nat. Geosci. 15, 609–614. https://doi.org/10.1038/s41561-022-00991-6

Faber, S., French, J.R., Jackson, R., 2018. Laboratory and in-flight evaluation of measurement uncertainties from a commercial Cloud Droplet Probe (CDP). Atmos. Meas. Tech. 11, 3645–3659. https://doi.org/10.5194/amt-11-3645-2018

Guo, S., Xue, H., 2021. The enhancement of droplet collision by electric charges and atmospheric electric fields. Atmos. Chem. Phys. 21, 69–85. https://doi.org/10.5194/acp-21-69-2021

Hobbs, P.V., Rangno, A.L., 1998. Microstructures of low and middle-level clouds over the Beaufort Sea. Q. J. R. Meteorol. Soc. 124, 2035–2071. https://doi.org/10.1002/qj.49712455012

Hou, T., Lei, H., He, Y., Yang, J., Zhao, Z., Hu, Z., 2021. Aircraft Measurements of the Microphysical Properties of Stratiform Clouds with Embedded Convection. Adv. Atmos. Sci. 38, 966–982. https://doi.org/10.1007/s00376-021-0287-8

Jayachandran, V., Nair, V.S., Babu, S.S., 2017. CCN characteristics over a tropical coastal station during south-west monsoon: observations and closure studies. Atmos. Environ. 164, 299–308. https://doi.org/10.1016/j.atmosenv.2017.06.012

Jose, S., Joseph, S., Lakshmi, N.B., 2026. Satellite based study on the role of Cloud Condensation Nuclei (CCN) and atmospheric thermodynamics in warm cloud evolution. Atmos. Res. 328, 108452. https://doi.org/10.1016/j.atmosres.2025.108452

Ke, Y., Wang, H., Yang, Y., Cui, Y., Shen, L., Wu, Z., Liu, S., Zhao, T., 2024a. A case study of aircraft observations of ice cloud microphysical properties over the North China Plain: Vertical distribution, vertical airflow and aerosol–cloud effects. Atmos. Res. 307, 107488.

https://doi.org/10.5194/egusphere-2026-4682
Preprint. Discussion started: 6 August 2026

https://doi.org/10.1016/j.atmosres.2024.107488

Kerminen, V.-M., Paramonov, M., Anttila, T., Riipinen, I., Fountoukis, C., Korhonen, H., Asmi, E., Laakso, L., Lihavainen, H., Swietlicki, E., Svenningsson, B., Asmi, A., Pandis, S.N., Kulmala, M., Petäjä, T., 2012. Cloud condensation nuclei production associated with atmospheric nucleation: a synthesis based on existing literature and new results. Atmos. Chem. Phys. 12, 12037–12059. https://doi.org/10.5194/acp-12-12037-2012

Khatri, P., Hayasaka, T., Holben, B.N., Singh, R.P., Letu, H., Tripathi, S.N., 2022. Increased aerosols can reverse Twomey effect in water clouds through radiative pathway. Sci. Rep. 12, 20666. https://doi.org/10.1038/s41598-022-25241-y

Khatri, P., Yoshida, K., Hayasaka, T., 2023. Aerosol Effects on Water Cloud Properties in Different Atmospheric Regimes. J. Geophys. Res. Atmos. 128, e2023JD039729. https://doi.org/10.1029/2023JD039729

Kleinheins, J., Shardt, N., Lohmann, U., Marcolli, C., 2025. The surface tension and cloud condensation nuclei (CCN) activation of sea spray aerosol particles. Atmos. Chem. Phys. 25, 881–903. https://doi.org/10.5194/acp-25-881-2025

Köhler, H., 1936. The nucleus in and the growth of hygroscopic droplets. Trans. Faraday Soc. 32, 1152–1161. https://doi.org/10.1039/TF9363201152

Lance, S., Brock, C.A., Rogers, D., Gordon, J.A., 2010. Water droplet calibration of the Cloud Droplet Probe (CDP) and in-flight performance in liquid, ice and mixed-phase clouds during ARCPAC. Atmos. Meas. Tech. 3, 1683–1706. https://doi.org/10.5194/amt-3-1683-2010

Lance, S., Nenes, A., Medina, J., Smith, J.N., 2006. Mapping the Operation of the DMT Continuous Flow CCN Counter. Aerosol Sci. Technol. 40, 242–254. https://doi.org/10.1080/02786820500543290

Lin, P.-H., Wang, S.-H., Klemm, O., Lin, N.-H., 2026. Separating the Twomey effect and the semi-direct effect in absorbing aerosol environments through the cloud-aerosol mixing ratio. Atmos. Chem. Phys. 26, 2083–2102. https://doi.org/10.5194/acp-26-2083-2026

Liu, A., Wang, H., Li, Y., Yin, Y., Li, B., Chen, K., Cui, Y., He, C., Dai, M., Liu, A., Wang, H., Li, Y., Yin, Y., Li, B., Chen, K., Cui, Y., He, C., Dai, M., 2020. Distribution Characteristics of Aerosol Size and CCN during the Summer on Mt. Tian and Their Influencing Factors. Atmosphere 11. https://doi.org/10.3390/atmos11090912

Liu, S., Wang, H., Zhao, D., Zhou, W., Du, Y., Zhang, Z., Cheng, P., Zhao, T., Ke, Y., Wu, Z., Huang, M., 2025. Measurement report: Aircraft observations of aerosol and microphysical quantities of stratocumulus in autumn over Guangxi Province, China – daylight variation, vertical distribution, and aerosol–cloud interactions. Atmos. Chem. Phys. 25, 4151–4165. https://doi.org/10.5194/acp-25-4151-2025

Lundberg, S.M., Lee, S.-I., 2017. A Unified Approach to Interpreting Model Predictions, in: Advances in Neural Information Processing Systems. Curran Associates, Inc.

Nair, A.A., Yu, F., Campuzano-Jost, P., DeMott, P.J., Levin, E.J.T., Jimenez, J.L., Peischl, J., Pollack, I.B., Fredrickson, C.D., Beyersdorf, A.J., Nault, B.A., Park, M., Yum, S.S., Palm, B.B., Xu, L., Bourgeois, I., Anderson, B.E., Nenes, A., Ziemba, L.D., Moore, R.H., Lee, T., Park, T., Thompson, C.R., Flocke, F., Huey, L.G., Kim, M.J., Peng, Q., 2021. Machine Learning Uncovers Aerosol Size Information From Chemistry and Meteorology to Quantify Potential Cloud-Forming Particles. Geophys. Res. Lett. 48, e2021GL094133. https://doi.org/10.1029/2021GL094133

Prabhakaran, P., Myers, T.A., Hoffmann, F., Feingold, G., 2025. Aerosol-Cloud Interactions in Marine Low-Clouds in a Warmer Climate. EGUsphere 1–26. https://doi.org/10.5194/egusphere-2025-2935

https://doi.org/10.5194/egusphere-2026-4682
Preprint. Discussion started: 6 August 2026

Tao, J., Kuang, Y., Ma, N., Hong, J., Sun, Y., Xu, W., Zhang, Y., He, Y., Luo, Q., Xie, L., Su, H., Cheng, Y., 2021a. Secondary aerosol formation alters CCN activity in the North China Plain. Atmos. Chem. Phys. 21, 7409–7427. https://doi.org/10.5194/acp-21-7409-2021

Thomas, L., Kumar, B., Zuend, A., Hassan-Barthaux, D., Rao, S.A., 2024. CCN activation in homogeneous isotropic turbulence: Response to particle characteristics and environmental conditions. Atmos. Res. 297, 107095. https://doi.org/10.1016/j.atmosres.2023.107095

Twomey, S., 1977. The Influence of Pollution on the Shortwave Albedo of Clouds. J. Atmos. Sci. 34, 1149–1152. https://doi.org/10.1175/1520-0469(1977)034%3C1149:TIOPOT%3E2.0.CO;2

Wang, N., Wang, Y., Lu, C., Zhu, B., Yan, X., Sun, Y., Xu, J., Zhang, J., Shen, Z., 2025. Interpretable ensemble learning unveils main aerosol optical properties in predicting cloud condensation nuclei number concentration. Npj Clim. Atmos. Sci. 8, 302. https://doi.org/10.1038/s41612-025-01181-y

Xu, X., Yin, J., Zhang, X., Xue, H., Gu, H., Fan, H., 2022. Airborne measurements of cloud condensation nuclei (*CCN*) vertical structures over Southern China. Atmos. Res. 268, 106012. https://doi.org/10.1016/j.atmosres.2021.106012

Zhang, M., Deng, X., Zhu, R., Ren, Y., Xue, H., 2021. The Impact of Aerosol Vertical Distribution on a Deep Convective Cloud. Atmosphere 12. https://doi.org/10.3390/atmos12060675

Zhang, R., Wang, Y., Li, Z., Wang, Z., Dickerson, R.R., Ren, X., He, H., Wang, F., Gao, Y., Chen, X., Xu, J., Cheng, Y., Su, H., 2022. Vertical profiles of cloud condensation nuclei number concentration and its empirical estimate from aerosol optical properties over the North China Plain. Atmos. Chem. Phys. 22, 14879–14891. https://doi.org/10.5194/acp-22-14879-2022

Zipfel, L., Andersen, H., Grosvenor, D.P., Cermak, J., 2024. How Cloud Droplet Number Concentration Impacts Liquid Water Path and Precipitation in Marine Stratocumulus Clouds—A Satellite-Based Analysis Using Explainable Machine Learning. Atmosphere 15. https://doi.org/10.3390/atmos15050596